Dual-Band Multi-Receiver Wireless Power Transfer: Architecture, Topology, and Control

Ming Liu, *Member, IEEE,* Minjie Chen, *Member, IEEE*
Department of Electrical Engineering
Andlinger Center for Energy and the Environment
Princeton University, Princeton, NJ, USA
Email: ml45@princeton.edu, minjie@princeton.edu

***Abstract*—Wireless power transfer (WPT) via near-field magnetic coupling is an enabling technology for many applications including consumer electronics and electric vehicles. A few WPT standards have been established with frequencies ranging from kHz to MHz. MHz operation offers smaller size and higher tolerance to coil misalignment, and kHz operation offers higher efficiency and higher power rating. This paper presents a WPT architecture with new transmitter and receiver topologies that are reconfigurable for dual-band operation. On the transmitter side, we developed a novel architecture based on the reactance steering network (RSN) which can seamlessly compensate an arbitrary load impedance for radio-frequency (RF) power amplifiers. It can transmit power at two frequencies (kHz and MHz range) with decoupled power modulation. On the receiver side, we developed a reconfigurable dual-band rectifier that can achieve a power density of 400 W/inch^3 at both 100 kHz and 13.56 MHz with very low component count. A dual-band reconfigurable WPT system comprising a dual-band transmitter and multiple dual-band receivers has been built and tested. The RSN-based dual-band transmitter can efficiently and simultaneously deliver 15 W of power to multiple receivers at both 100 kHz and 13.56 MHz.**

***Index Terms*—dual-band wireless power transfer, reactance steering network, high frequency power conversion.**

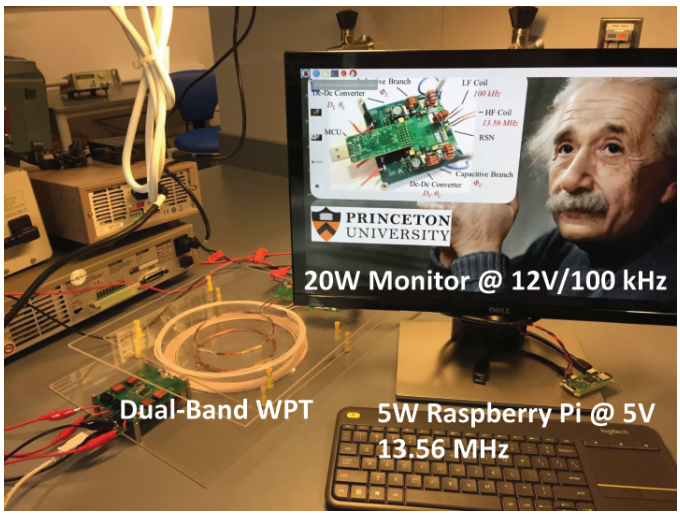

Fig. 1. A dual-band wireless powered desktop at Princeton Powerlab. The system simultaneously powers a 5 W Raspberry Pi at 13.56 MHz and a 20 W monitor at 100 kHz. The full desktop is completely wireless: it is wireless powered and wireless connected to the Internet.

I. Introduction

Wireless power transfer (WPT) through near-field magnetic coupling is an enabling technology for many applications ranging from consumer electronics to electric vehicles [1]–[4]. A few WPT standards have been established (e.g., AirFuel, Qi) with frequencies ranging from hundreds of kHz to a few MHz. These standards may merge and may cover many frequency domains in the future. In general, there is a fundamental tradeoff between kHz operation and MHz operation in WPT: MHz operation enables long distance power transfer and better robustness against coil misalignment [5], while kHz operation offers higher efficiency and higher power transfer capability [6]. Both kHz and MHz WPT standards will co-exist for a long period of time [7]. High performance transmitters that can power multiple receivers at different frequencies, and high performance receivers that can receive power from a variety of transmitters are the main focus of this paper.

Fig. 1 shows a demo system at Princeton Powerlab where a dual-band transmitter simultaneously powers a 5 W Raspberry Pi at 13.56 MHz and powers a 20 W monitor at 100 kHz. Fig. 2 shows the coil placement diagram. The transmitting coils and the receiving coils may be loosely coupled or closely coupled. The load impedance on the transmitter side may change across a wide range. The transmitter needs to maintain high performance at both kHz and MHz, and the receivers may need to receive power from multiple frequencies (i.e., one receiver is compatible with multiple standards).

Transmitter solutions for WPT at 100 kHz are mature. Full-bridge-inverter-based topologies are widely considered as popular options at 100 kHz. For MHz operation, maintaining resistive load for high frequency inverters (e.g., Class-E [8]) is critical to achieve high efficiency and high power rating. There exist many design techniques that can compress load resistance variation for single-switch MHz inverters [9]–[11]. However, for reactance variation, the most commonly-adopted solution is to use a separate tunable matching network (TMN) [12]. [13] presents a variable reactance rectifier which helps to address the challenge from the receiver side. The additional passive components and switching devices in these designs increase the volume, reduce the efficiency and increase the cost. Moreover, the resolution of these compensation methods depends on the number of components used in the matching network. Precise and seamless reactance compensation is not achievable, especially with significant reactance variation.

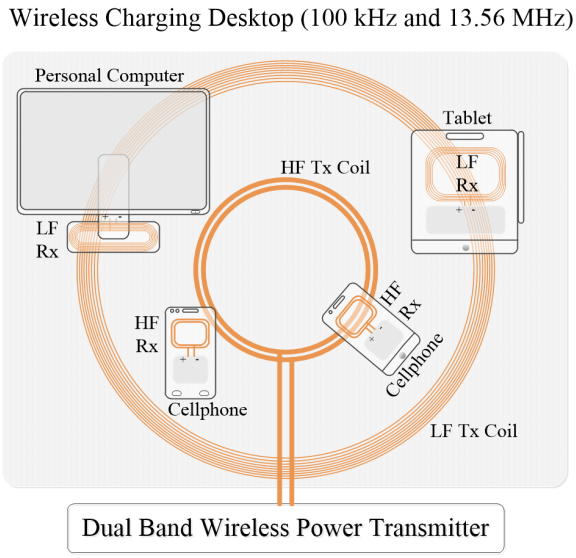

Fig. 2. Coil placement of a dual-band WPT desktop with multiple receivers operating at different frequencies with different power ratings.

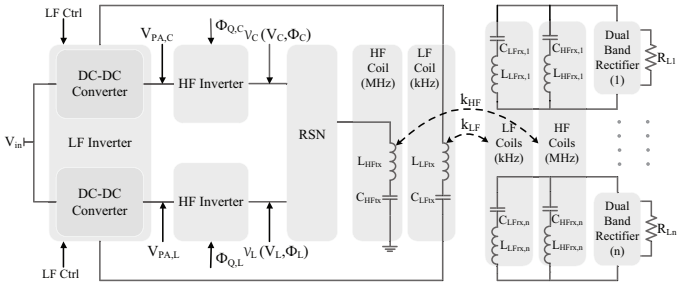

Fig. 3. Block diagram of a dual-band WPT system comprising one RSN transmitter and multiple dual-band reconfigurable receivers with different coupling coefficients.

Similarly, receiver solutions for WPT at 100 kHz are mature. Synchronous rectified full-bridge topology can offer high efficiency and high tolerance to impedance variation. For MHz operation, Class-E based receifier topologies are highly competitive as they offer high performance with low component count and low electromagnetic interference (EMI). Since the receivers are usually co-packaged with portable devices or in electric vehicles with size and thermal limits, low component count and small size are highly preferred [14].

This paper presents a dual-band WPT architecture with novel solutions on both the transmitter side and the receiver side. On the transmitter side, we developed a reactance steering network (RSN) based dual-band transmitter which can independently modulate the power transmitted at two frequencies [15]. Instead of merging two independent single-frequency transmitters together, the RSN architecture reuses the components and creates mutual advantages at two frequencies to improve the performance. The RSN mechanism ensures high performance operation of the Class-E inverter across a very wide load impedance range. On the receiver side, we deveoped a reconfigurable dual-band receiver that can maintain high performance at both frequencies with very low component count. The receiver functions as a synchronous half-bridge rectifier at 100 kHz, and functions as two series-stacked Class-E rectifiers at 13.56 MHz. The two active switches and many passive components are reused at both frequencies. The transmitter and the receiver are merged as one WPT system that can operate at two frequencies while maintaining high performance. The prototyped RSN transmitter can deliver 15 W of power to multiple dual-band receivers with >70% efficiency at 13.56 MHz, and >80% efficiency at 100 kHz with significant coil misalignment.

The remainder of this paper is organized as follows: Section II provides an overview of the dual-band WPT system. The topology and operation principles of the RSN-based dual-band transmitter are presented in Section III. Section IV introduces the topology and operation principles of the reconfigurable dual-band receiver. Section V presents the prototype and experimental results, including detailed theoretical analysis and measured results of the dual-band transmitter and receiver. Finally, Section VI concludes this paper.

II. Dual-Band Multi-Receiver WPT System

Fig. 3 shows the block diagram of the proposed dual-band WPT system with a RSN based transmitter, and multiple reconfigurable dual-band receivers. The RSN transmitter comprises two LF dc-dc converters operating at kHz (e.g., 100 kHz), two HF inverters operating at MHz (e.g., 13.56 MHz), a RSN, a LF transmitting coil, and a HF transmitting coil. The receiver side comprises an active dual-band receiver and multiple single-band rectifiers. The two dc-dc converters modulate the inputs of the HF inverters, and simultaneously drive the LF transmitting coil at 100 kHz. By modulating the voltage amplitude and the phase of the two HF inverters following a "reactance-steering" approach [15], the two HF inverters see pure resistive load. The dc-dc converters also drive the LF transmitting coil as a phase-shift full bridge, transferring power at both LF and HF simultaneously.

Each of the function block in the RSN transmitter can be implemented in multiple ways: the LF inverters can be implemented as Class-D or full-bridge inverters; the low-pass filters at the output of the LF inverters can be implemented as L-networks or π-networks; the HF inverters can be implemented as Class-E, Class-F or Class-Φ inverters; the RSN can be implemented as a three-port LC network or other three-port network types. The LF and HF transmitting and receiving coils are standard coils tuned for nominal coupling coefficients. The two half-bridges drive the LF coil, and the HF inverters drive the HF coil. The power delivered at the two frequencies can be modulated independently.

The receiver developed in this paper is a dual-band reconfigurable receiver that can function at either 100 kHz or 13.56 MHz. A single dual-band receiver can be reprogrammed to function at either frequency, and multiple receivers working at different frequencies can be placed in adjacent to each other while all maintaining high performance. The transmitter sees the impedance of all receivers operating at two frequencies with their power adds together.

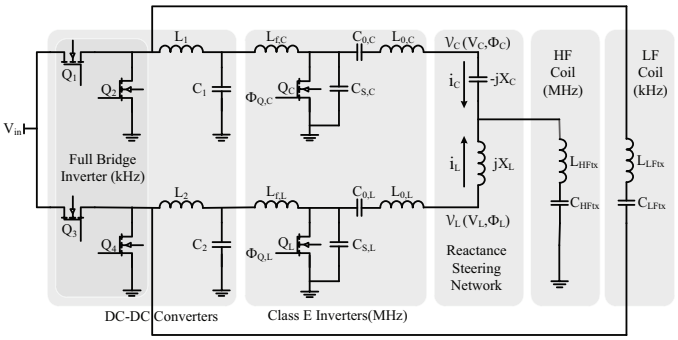

Fig. 4. Schematic of an example dual-band transmitter comprising a RSN, two Class-E PAs, two buck converters and two transmitting coils.

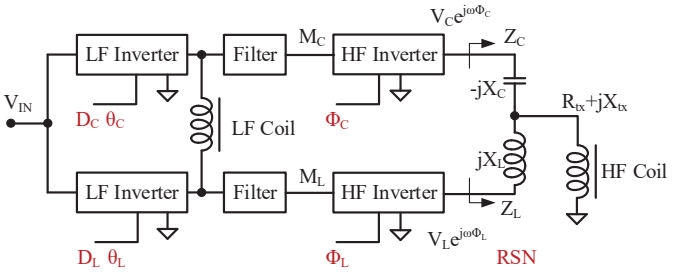

Fig. 5. Simplified block diagram of the RSN architecture. This architecture has six input variables: D_C, D_L, θ_C, θ_L, Φ_C, Φ_L, and independently drives two coils at two frequencies.

III. Dual-Band RSN Transmitter

Fig. 4 shows the schematic of an example implementation of the RSN based dual-band transmitter with two half-bridge LF inverters, two LC low pass filters, and two Class-E HF inverters. The two half-bridge inverters and the two low-pass filters function as two buck converters that modulate the inputs of the two Class-E inverters. The two Class-E inverters are loaded with a LC resonant network including an inductive branch jX_L and a capacitive branch $-jX_C$. The two half-bridge inverters also drive a low frequency coil as a full bridge inverter. The power transferred at the two frequencies can be individually modulated depending on the load conditions.

A. High Frequency Operation of the Dual-Band Transmitter

Detailed operation principles and design guidelines of the RSN architecture have been presented in [15]. As illustrated in Fig. 5, the main concept of the RSN architecture is to split the power flow in a two-branch L-C network to compensate the load reactance variation seen by the HF transmitter. With accurate amplitude and phase modulation, the load impedance of the two HF inverters can be maintained pure resistive across a very wide load impedance range. The core function block of the RSN architecture is the three terminal network comprising jX_L and $-jX_C$. The input impedance of the transmitter coil is (Z_{tx} = R_{tx} + jX_{tx}). The phase and amplitude of the output of the two HF inverters, ($V_C e^{j\omega\Phi_C}$, $V_L e^{j\omega\Phi_L}$), should be precisely controlled depending on the load impedance:

- If Z_{tx} is resistive, the two HF inverters equally share power and both see pure resistive load;
- If Z_{tx} is inductive, the system steers power towards the capacitive branch. The capacitive element $-jX_C$ is used to compensate the inductive load Z_{tx};
- If Z_{tx} is capacitive, the system steers power towards the inductive branch. The inductive element jX_L is used to compensate the capacitive load Z_{tx};
- By adjusting the ratio between V_L and V_C, and the phase difference between Φ_L and Φ_C, the reactance used for compensation at each branch can be precisely controlled to maintain resistive load for both HF inverters.

The RSN can be implemented in many different ways. Compared to a conventional tunable matching network with discrete compensation elements, the proposed RSN architecture has the following advantages:

- It can seamlessly compensate an arbitrary load impedance range and maintain pure resistive load;
- It requires very few additional component compared to a conventional TMN design;
- It has smooth transient behavior without mode-switching spikes or harmonics;
- The dc-dc converters in the RSN architecture can be used to drive a LF transmitter with no additional components.

The power modulation of the RSN architecture is achieved by adjusting the amplitude of the dc-dc converters, or tuning the phases of the HF inverters.

Online impedance estimation enables maximum efficiency tracking and maximum power point tracking for WPT. The load impedance can be rapidly estimated without using current sensors. Based on the analysis in [15], the input power of the two inverter branches, P_C and P_L, are

$$\begin{cases} P_C = \frac{V_C^2(R_{tx}-K_{LC}(R_{tx}\cos(\Delta_{LC})-X_{tx}\sin(\Delta_{LC})))}{2X_O^2} \\ P_L = \frac{V_L^2(R_{tx}-\frac{1}{K_{LC}}(R_{tx}\cos(\Delta_{LC})+X_{tx}\sin(\Delta_{LC})))}{2X_O^2} \end{cases} . \quad (1)$$

The ratio of the power delivered by the two branches is:

$$\frac{P_L}{P_C} = K_{LC}^2 \frac{\eta_C(R_{tx}-\frac{1}{K_{LC}}(R_{tx}\cos(\Delta_{LC})+X_{tx}\sin(\Delta_{LC})))}{\eta_L(R_{tx}-K_{LC}(R_{tx}\cos(\Delta_{LC})-X_{tx}\sin(\Delta_{LC})))}. \quad (2)$$

Here η_L and η_C are the efficiencies of the two dc-dc converters. Eq. (2) indicates that the load impedance R_{tx} and X_{tx} are closely related to the input dc power ratio $\frac{P_L}{P_C}$ for a given η_L, η_C, K_{LC}, and Δ_{LC}. $\frac{P_L}{P_C}$ can be easily measured from the dc-dc converters with simple circuit and low cost. Fig. 6 shows the relationship of the input dc power ratio P_L/P_C and input impedance $Z_{tx} = R_{tx} + jX_{tx}$ when $K_{LC} = 1$ and $\Delta_{LC} = 90°$. The load resistance can be estimated with the total load power $P_L + P_C$ and the voltage amplitudes. Assume the efficiencies of the two inverters are the same, the load input impedance Z_{tx} can be estimated with P_L/P_C. With different η_L and η_C, the one-to-one mapping relationship can be found through experiments.

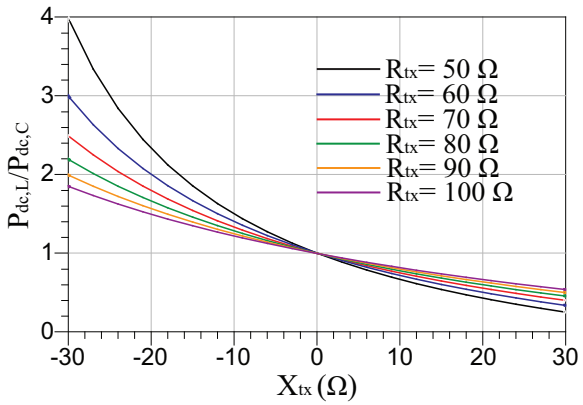

Fig. 6. Power ratio P_L/P_C as a function of the load impedance Z_{tx}. This power ratio can be used to perform online load impedance estimation.

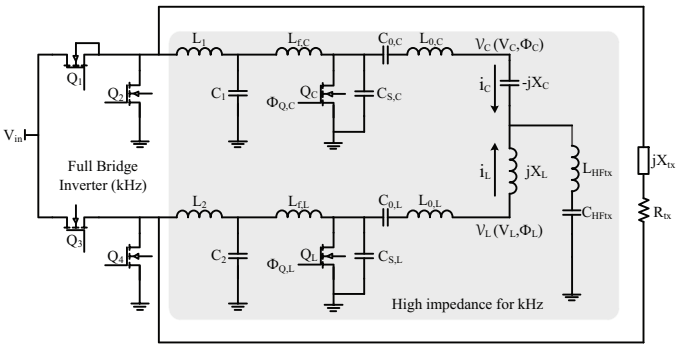

Fig. 7. Schematic of the dual-band transmitter with a phase-shifted full bridge LF transmitter, and a RSN-based HF transmitter. The two high frequency inverters look like two high impedance loads for the full bridge inverter.

B. Low Frequency Operation of the Dual-Band Transmitter

One way to implement the two dc-dc converters is to build them as two buck converters with two half-bridge inverters (Fig. 5). The two half-bridge inverters can drive a LF coil as a phase-shifted full bridge, while at the same time modulate the dc voltages M_C and M_L for the HF inverters. The LF power transfer is controlled by the phase of the two LF inverters θ_L and θ_C. The output M_L and M_C are controlled by D_L and D_C. Fig. 7 shows the schematic of the dual-band transmitter with the RSN high frequency transmitter shaded. Here R_{tx} and X_{tx} are the resistance and reactance of the low frequency coils. In this circuit, Q_1 and Q_2 operate as one phase-shifted half-bridge, and Q_3 and Q_4 operate as the other phase-shifted half-bridge. The duty ratios of of the two half-bridges modulate M_C and M_L, and the phase difference between the two half-bridges modulates the power output of the LF transmitter.

Benefiting from the low pass filters at the output of the dc-dc converters and the input inductors of the Class-E inverters, the LF transmitter and the HF transmitter are well-decoupled from each other. θ_C and θ_L modulate the LF transmitter, but have no impact on M_C and M_L, and thus have no impact on the HF transmitter. Similarly, Φ_C and Φ_L modulate the HF transmitter, but have no impact on the LF transmitter. When D_C and D_L are adjusted to modulate M_C and M_L, θ_C and θ_L should be changed accordingly to maintain the power levels of the LF transmitter. Similar to [3], the two overlapped transmitter coils and the related resonant tanks are optimally tuned for 100 kHz and 13.56 MHz, respectively.

TABLE I
PARAMETERS OF THE EXAMPLE DUAL-BAND RECTIFIER

L_{f1}	C_{r1}	L_{f2}	C_{r2}	C_{f1}	C_{f2}
1.2 μH	500 pF	1.2 μH	500 pF	20 μF	20 μF

IV. DUAL-BAND RECONFIGURABLE RECEIVER

In many application scenarios, a wireless power receiver may need to be compatible with multiple standards. The receivers also need to be compact and efficient with low component count. A full bridge synchronous rectifier can work at both high frequencies and low frequencies. However, the square-wave harmonic contents of the full bridge rectifier raise concerns for many portable applications. It is also difficult to drive the high side switch of a full-bridge rectifier. One can use Class-E rectifiers at high frequencies to reduce the harmonic contents, but the inductance of the chock inductor is large and is usually not acceptable.

Fig. 8 (a) shows the topology of a dual-band reconfigurable receiver. The rectifier comprises two switches Q_{r1} and Q_{r2}, two shunt capacitors C_{r1} and C_{r2}, two RF chock inductors, two filter capacitors, and one switch Q_s for HF/LF mode selection. The dual-band rectifier can either work in the kHz range (e.g., 100 kHz), or work in the MHz range (e.g., 13.56 MHz), depending on if Q_S is on or off. The parasitic capacitance of the diodes are absorbed into the shunt capacitors. Table II lists the component values of the proposed dual-band reconfigurable rectifier.

Fig. 8 (b) and (c) illustrates the operation principles of the proposed rectifier in HF and LF, respectively. If switch Q_s is kept on, the rectifier functions as two Class-E half-wave rectifiers stacked in series. The rectifier receives power from the high frequency coil (i.e., 13.56 MHz). If switch Q_s is kept off, the rectifier functions like a Class-D rectifier and receives power from the low frequency coil (i.e., 100 kHz). As shown in Fig. 8 (c), the RF chock inductors (L_{f1} and L_{f2}) can be considered as short, and the shunt capacitors (C_{r1} and C_{r2}) can be considered as open. Q_s can be implemented as a low-speed switch in the controller IC. The frequency gap between 100 kHz and 13.56 MHz is large enough to size this inductor, so that it looks like a short at 100kHz.

Fig. 9 (a) and (b) show the simulated voltage waveforms of Q_{r1} and Q_{r2} working at 13.56 MHz and 100 kHz, respectively. At high frequencies, the rectifier function as two Class-E rectifiers stacked in series and the waveform of the voltage across the switches is half-wave sinusoidal. At low frequencies, the rectifier function as one Class-D rectifier and the voltage across the switches is rectangular. In 100 kHz operation, the shunt capacitors may resonate with the RF chock inductors, resulting in a high frequency ripple at V_{rec}. One can reduce the oscillation by using a small C_r at the cost of higher distortion at 13.56 MHz or using a small L_f at the cost of higher ac current across the inductors. Fig. 9 (c) and (d) show the simulated voltage waveforms of the current

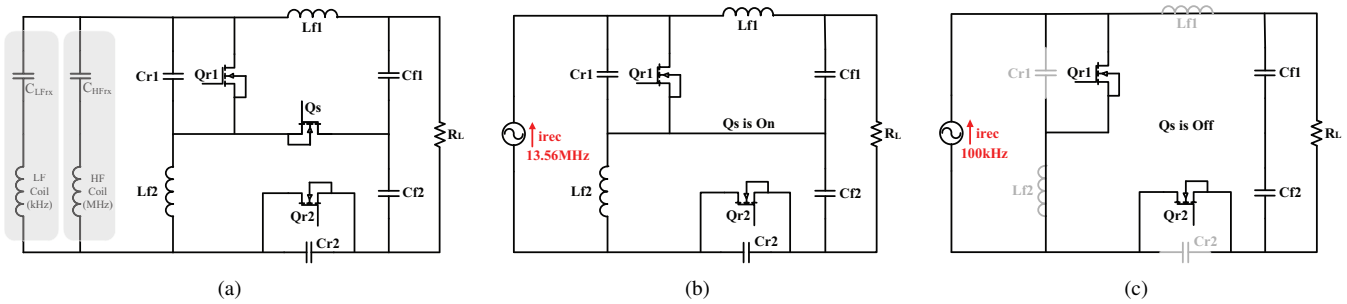

Fig. 8. Circuit topology of a dual-band rectifier: (a) full schematic of the dual-band rectifier, (b) schematic of the transmitter when it operates at high frequency with Q_S kept on, (c) schematic of the transmitter when it operates at low frequency with Q_S kept off.

and voltage of the mode selection switch at 13.56 MHz and 100 kHz, respectively. The dashed lines are the dc output current and dc output voltage, respectively. The peak current flow through Q_1 and Q_2 is twice of the dc output current. The voltage across the mode selected switch is same as that of the switch Q_r, which can be used to choose the current and voltage rating of the switch.

Fig. 9 (e) and (f) shows the simulated results of the total harmonic distortion and the ratio of the switch peak voltage to the output voltage (the voltage stress of Q_1 and Q_2), and the input impedance of the dual-band rectifier with different C_r values. The THD and the switch voltage stress can be reduced by increasing the C_r value. However, a higher C_r will reduce the input resistance of the rectifier, which may increase the conduction loss of the receiving coil, the RF chock inductor, and the switches on the receiving side.

The design principles of the dual-band rectifier are:

- The shunt capacitor C_r should be designed depending on the THD requirement, voltage stress, and the ac self-resistance of the receiving coil;
- The model selection switch Q_S should be implemented as a low-speed switch with low on-resistance. Its voltage rating is the same as the two high speed switches Q_r;
- The inductors should be designed so that they function as RF chock inductors at high frequencies and function as shorts at low frequencies;
- The ouput filter capacitor C_f should be big enough to eliminate the output voltage ripple.

At high frequencies (e.g., 13.56 MHz), the optimal duty ratio of the switches in the dual-band rectifier depends on the load impedance. Fig. 10 (a) and (b) show the optimal duty ratio and voltage stress of the switches for a range of R_L. The optimal duty ratio decreases as R_L increases. Since the dual-band rectifier function as two series-stacked Class-E half-wave current-driven rectifier, the voltage stress of each high frequency switch is only one half of the voltage stress of a conventional Class-E current-driven rectifier. For low frequency operation, the voltage stress of the two switches is identical to that of a half bridge rectifier. Fig. 10 (c) and (d) shows the simulated total harmonics distortion (THD) of the dual-band rectifier and the full bridge rectifier operating at 13.56 MHz. As expected, the dual-band reconfigurable rectifier works as two series-connected Class-E rectifiers and offers significantly lower THD than a full bridge rectifier.

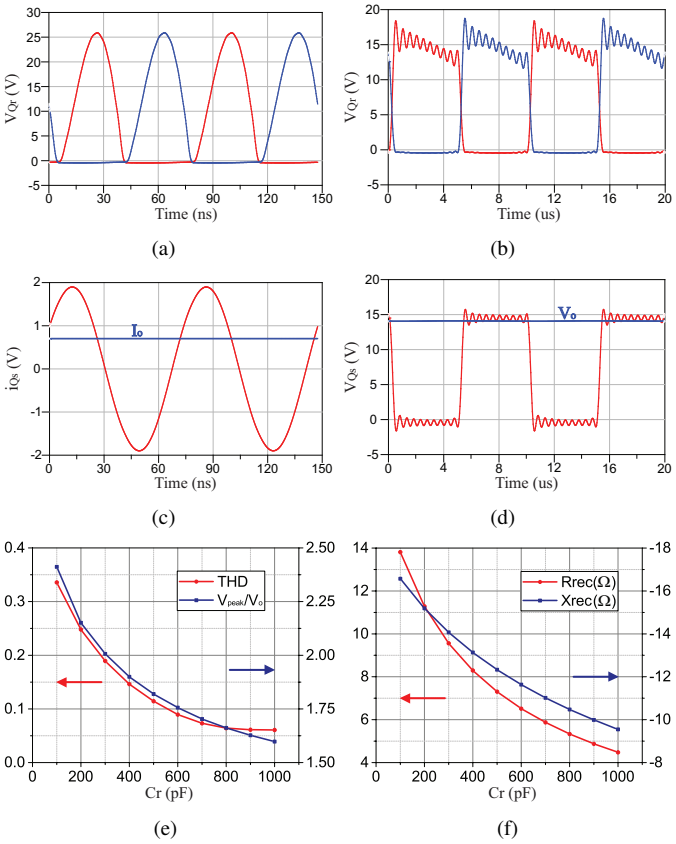

Fig. 9. (a) simulated drain-to-source voltage of Q_r at 13.56 MHz, (b) simulated drain-to-source voltage of Q_r at 100 kHz, (c) simulated current waveform of the mode selection switch Q_S at 13.56 MHz, (d) simulated voltage waveform of the mode selection switch Q_S at 100 kHz, (e) simulation total harmonic distortion and the ratio of the switch peak voltage to its output voltage, (f) simulated rectifier input impedance.

Comparing to a system with two separate rectifiers, the advantages of the proposed dual-band rectifier include:

1) Higher efficiency, lower voltage stress, and lower harmonic distortion than a full bridge rectifier at 13.56 MHz.
2) Higher efficiency and *Qi* compatibility at 100 kHz (drive a low frequency coil with two half-bridge inverters).
3) Very low component count (the dual-band system has the same component count as a push-pull Class-E rectifier).
4) Simple sensing, control and gate drive circuitry. The HF and LF sensing and control circuitry, as well as the mode-selection switch can be implement in a single chip.

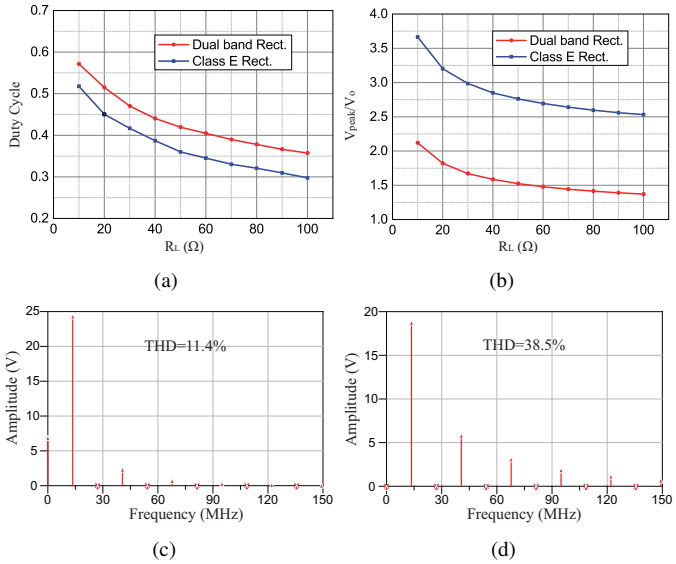

Fig. 10. (a) Simulated rectifier duty cycle at 13.56 MHz; (b) Simulated switch voltage stress at 13.56 MHz; (c) Simulated total harmonic distortion of the dual-band rectifier at 13.56 MHz; (d) Simulated total harmonic distortion of the full bridge rectifier at 13.56 MHz.

In summary, the proposed dual-band rectifier is a promising candidate for future practical design where high performance and low component count are needed. The key principles of this rectifier is to merge high efficiency low frequency rectifiers (e.g., Class-D) with low distortion high frequency rectifiers (e.g., Class-E), without increasing the component count and the device stress. When designing this rectifier, the LF rectifier and HF rectifier should be jointly optimized so that they share the same loss budget when delivering the same amount of power with the same thermal limit.

V. Experimental Verification

Fig. 11 shows a prototype dual-band WPT system comprising a 100 kHz transmitter, a 13.56 MHz transmitter, a 100 kHz receiver, and two 13.56 MHz receivers. The dual-band transmitter is shown in Fig. 12. The component values of the dual-band transmitter are listed in Table II. The input inductors of the two Class-E inverters, $L_{f,C}$ and $L_{f,L}$, are designed to resonant with the shunt capacitors, $C_{S,C}$ and $C_{S,L}$, following the method described in [11]. The resonant frequency of the output tank of the two Class-E inverters, $L_{0,C}$ and $C_{0,C}$, $L_{0,L}$ and $C_{0,L}$, are 13.56 MHz. The two HF switches are implemented as GaN transistors (GS66504B). The output capacitance of the two HF switches (about 60 pF) are absorbed into the shunt capacitors $C_{S,C}$ and $C_{S,L}$. Fig. 14 shows the ZVS operation of the HF switches with Z_{tx} (= $14 - j26\ \Omega$). The system delivers 10 W with and without RSN at 13.56 MHz.

A 100 kHz receiver and a 13.56 MHz receiver are designed and tested to evaluate the performance of the dual-band transmitter. The dual-band rectifier shown in Fig. 13 is used as the 100 kHz receiver when Q_S is on and as the 13.56 MHz receiver when Q_s is off, respectively. The diameters of the HF coil and the LF coil are 10 cm and 20 cm, respectively. The distance between the transmitting coil and the receiving

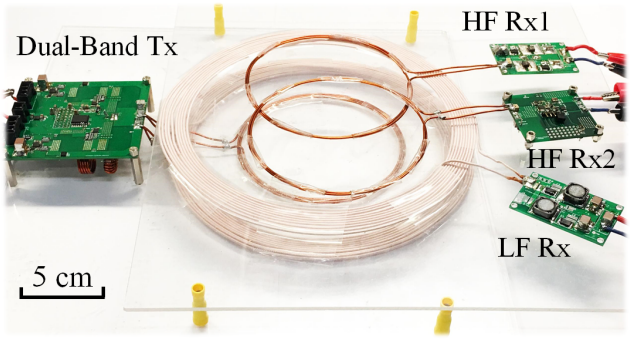

Fig. 11. The prototype dual-band WPT system with a RSN transmitter, a pair of HF coils, a pair of LF coils, and three reconfigurable receivers.

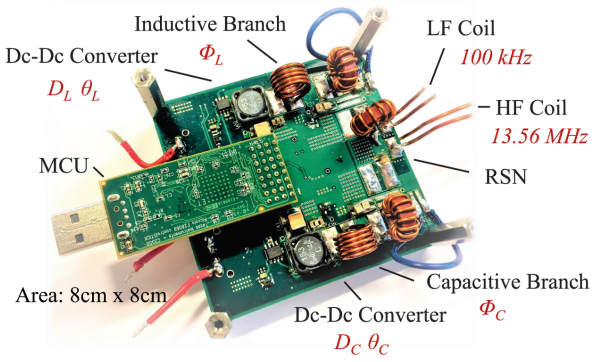

Fig. 12. The dual-band transmitter with an inductive branch, a capacitive branch, a microcontroller (TI F28069), and a reactance steering network.

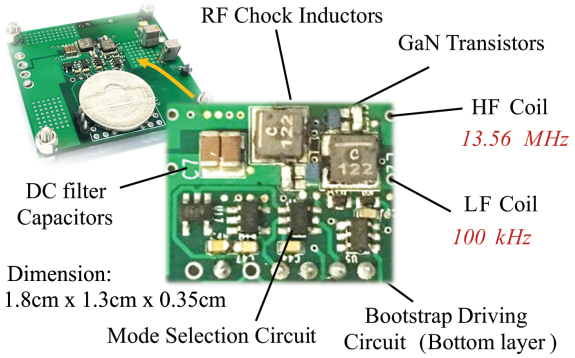

Fig. 13. The active dual-band rectifier with two GaN transistors, the mode selection and bootstrap driving circuits. The power density is 400 W/inch^3.

TABLE II
PASSIVE COMPONENT VALUES OF THE DUAL-BAND TRANSMITTER.

$L_{f,C}$ 200 nH	$L_{0,C}$ 1650 nH	$C_{S,C}$ 260 pF	$C_{0,C}$ 83 pF	C_{RSN} 397 pF	C_1 20 uF	L_1 10 uH
$L_{f,L}$ 200 nH	$L_{0,L}$ 1650 nH	$C_{S,L}$ 260 pF	$C_{0,L}$ 83 pF	L_{RSN} 350 nH	C_2 20 uF	L_2 10 uH

coils is 2.8 cm. The maximum horizontal misalignment is 5 cm. Fig. 15 shows the measured end-to-end efficiency of the 100 kHz WPT system the 13.56 MHz WPT system with and without using the RSN. As shown in Fig. 15, the system with the RSN achieves higher efficiency than the system without

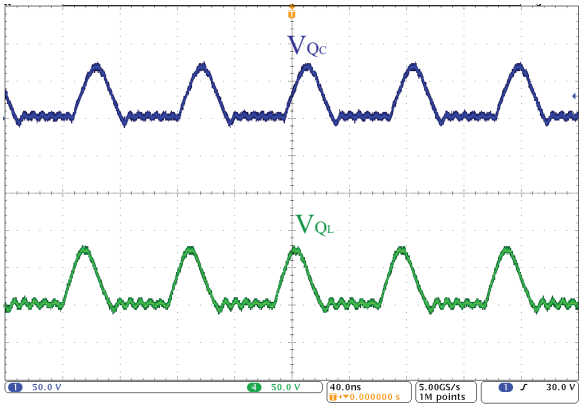

(a)

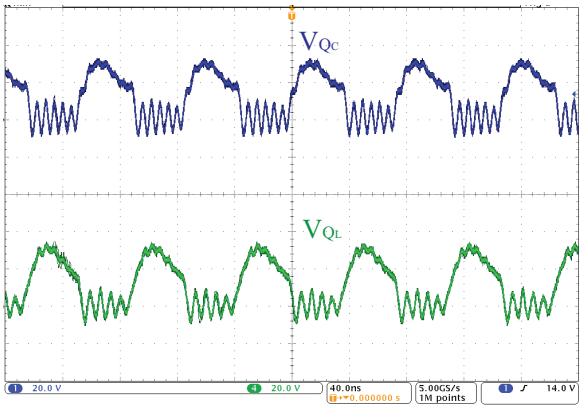

(b)

Fig. 14. Measured drain-to-source voltage of the two HF switches: the switches are (a) soft-switched with RSN operation, (b) hard-switched without RSN operation.

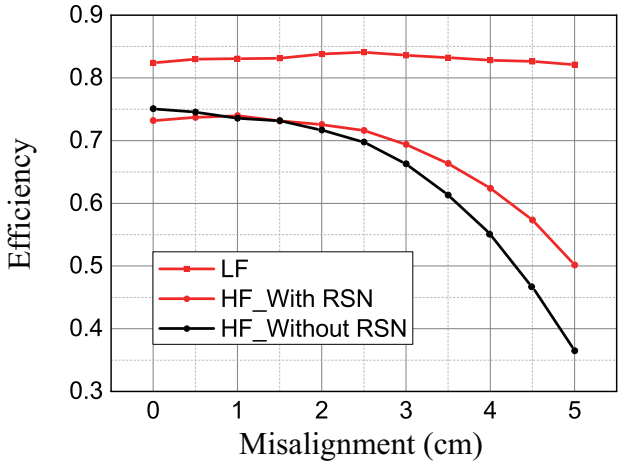

Fig. 15. Measured end-to-end efficiency of the dual-band WPT system as a function the coil misalignment. The radius of the HF coil is 5 cm, and the radius of the LF coil is 10 cm.

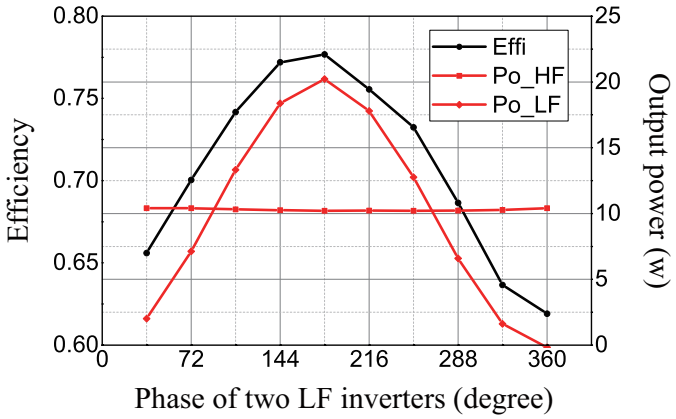

Fig. 16. The system can maintain a constant power for the high frequency coil (Po_HF) and modulate the power of the low frequency coil (Po_LF).

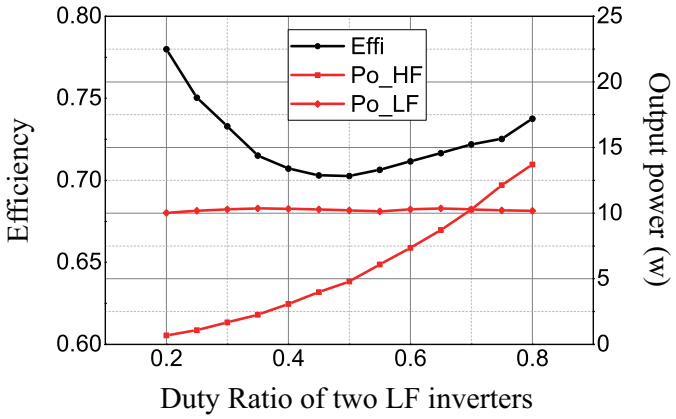

Fig. 17. The system can maintain a constant power for the low frequency coil (Po_LF) and modulate the power of the high frequency coil (Po_HF).

the RSN across the entire misalignment range. With the higher load reactance, (e.g., at the misalignment of 5 cm), the efficiency improvement is up to 13%. Note the low efficiency of the HF operation under the large misalignment is caused by the high ESR of the HF coil. The LF coil also interacts with the HF coil at 13.56 MHz, which further decrease the system efficiency with large misalignments.

Fig. 16 and Fig. 17 show the experimental results with the LF and HF systems working together. The prototype dual-band WPT system can independently controlling the output power of the LF transmitter and HF transmitter. The power delivered by the LF transmitter is controlled by the duty ratio D_L, D_C, and the phase shift θ_L and θ_C. The power delivered by the HF transmitter is controlled by the intermediate voltage M_L, M_C, and the phase Φ_L and Φ_C. The operation of the two frequency bands are independent from each other with negligible cross-coupling effects. As shown in Fig. 16, by keeping D_L, D_C, Φ_L, Φ_C as constants, and modulating the phase difference between θ_L and θ_C form 0 to 2π, the power transferred at 100 kHz (Po_LF) can be modulated between 0 W to 20 W, and the power transferred at 13.56 MHz (Po_HF) can be kept constant at 10 W. Similarly, as shown in Fig. 17, one can keep the power transferred at 13.56 MHz constant at 10 W, and modulates the power transferred at 100 kHz from 0 W to 15 W by changing the duty ratio of the LF inverters. The measured efficiencies of the HF and LF transmitters working together are shown in Fig. 16 and Fig. 17, respectively. When delivering 10 W of power at 13.56 MHz, and delivering 20 W of power at 100 kHz, the system reaches a maximum end-to-end efficiency of 77.7%.

Fig. 18 (a) shows the estimated transmitting coil input

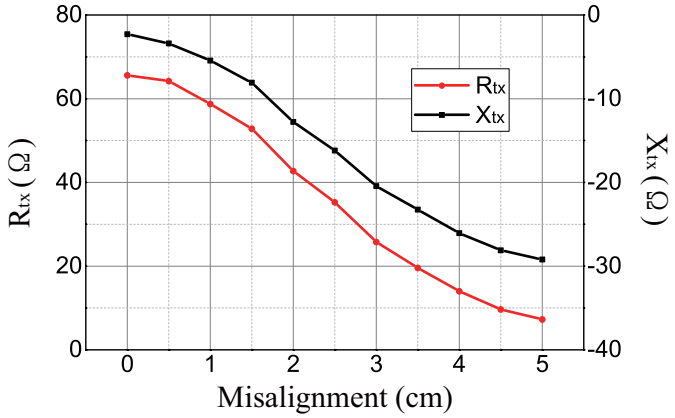

(a)

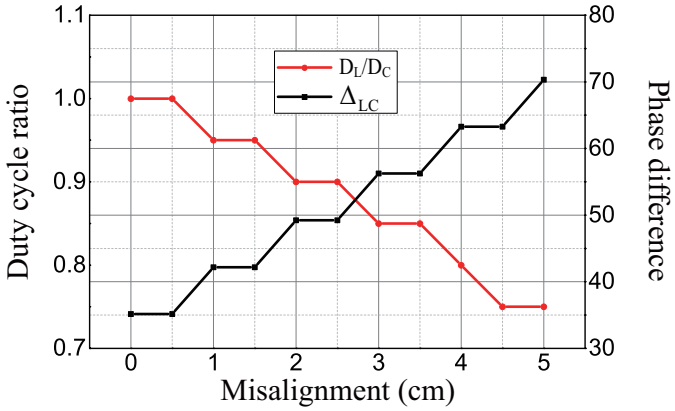

(b)

Fig. 18. Experimental results with the coil misalignment changing from 0 cm to 5 cm: (a) estimated R_{tx} and X_{tx}, (b) duty cycle ratio D_L/D_C and phase difference Δ_{LC} with online impedance estimation.

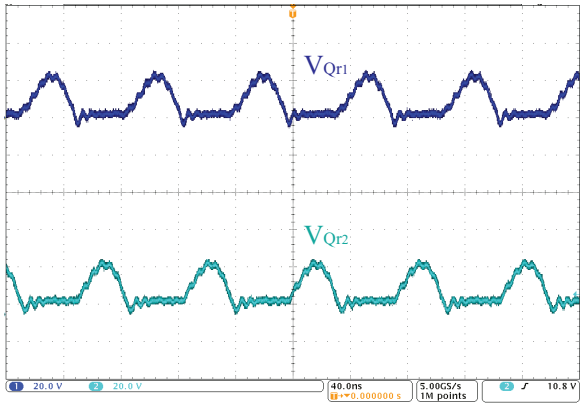

(a)

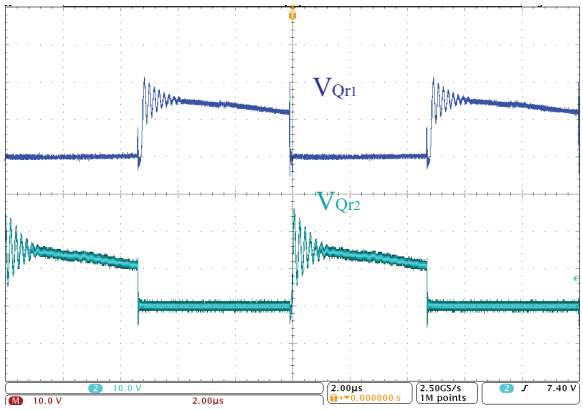

(b)

Fig. 19. The active dual-band rectifier and measured waveforms: (a) drain-source waveform at 13.56 MHz, (b) drain-source waveform at 100 kHz.

impedance Z_{tx} = R_{tx}+jX_{tx}. Here the impedance variation of Z_{tx} is created by tuning the coil misalignment from 0 cm to 5 cm. Fig. 18 (b) shows the control parameters of the power ratio based control. Here D_L/D_C is the ratio of the duty cycle of the L branch and the C branch buck converter. Δ_{LC} is the phase difference between the driving signal of the L branch switch Q_L and the driving signal of the C branch switch Q_C. The control parameters are selected from a look-up table.

In order to further improve the system end to end efficiency, a dual-band rectifier implemented with GaN switches is built and tested (Fig. 8). Note the dual-band rectifier used in the previous experiment employs the passive diodes. Fig. 13 shows the synchronous rectifier. Here the effective dimension of the active rectifier is about 1.8 cm $\times$ 1.3 cm. The driving and auxiliary circuitry are included. Based on the analysis in Section IV, the shunt capacitors of the dual-band rectifier C_{r1} and C_{r2} are 500 pF and the ratio V_{peak}/V_o is about 1.82 (Fig. 9). The maximum dc output voltage of Q_{r1} and Q_{r2} (V_{DS}=40 V) is about 22 V and the maximum output power is 20 W at 13.56 MHz. A low cost and low on-resistance MOSFET ECH8420 is used as the mode selection switch Q_S. The RF chock inductors L_{r1} and L_{r2} are chosen as 1.2 μH which behave as high impedance (about 102j Ω) at 13.56 MHz to block the high frequency current (reduce the ac power loss). They behave as short at 100 kHz. Fig. 19 (a) and (b) show the experimental waveforms for the dual-band rectifier when working at HF and LF, respectively. The measured waveforms closely match with simulations in Fig. 9 (a) and (b). The ringings on the rectifier input voltage at 100 kHz is caused by the inductors L_{f1} and L_{f2} used for high frequency rectification.

Fig. 20 (a) shows the measured dc-dc efficiency of the WPT system with active and passive rectifiers at 13.56 MHz, respectively. Fig. 20 (b) shows the measured system efficiency of the active and passive dual-band rectifier when they are working at 100 kHz. The efficiency of the dual-band WPT system with the active rectifier is significantly higher than that of the system with passive rectifier across the full power range.

VI. Conclusions

A dual-band WPT architecture targeting multi-receiver applications with significant coil misalignment and load variation is presented in this paper. This architecture is developed based on a novel reactance steering network (RSN) that can precisely compensate an arbitrary load reactance by dynamically steering the reactive power between two inverter branches. We developed the theory of RSN and presented a design method that can cover an arbitrary reactance variation range. This paper also presents the topology and operation principles

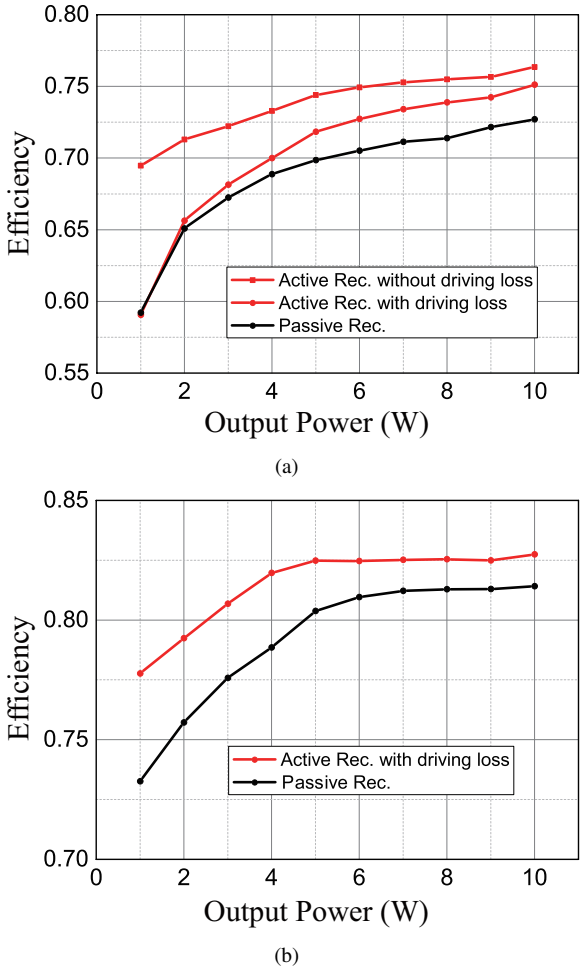

Fig. 20. Active and pssive rectifier efficiency: (a) efficiencies at 13.56 MHz, (b) efficiencies at 100 kHz.

of a dual-band reconfigurable rectifier that can achieve high performance at both 100 kHz and 13.56 MHz. The dual-band transmitter and the reconfigurable rectifier are experimentally verified by a dual-band WPT system that can efficiently and independently power multiple 100 kHz and 13.56 MHz receivers with significant coil misalignment and load variation.

ACKNOWLEDGMENT

The authors would like to thank Andlinger Center for Energy and the Environment at Princeton University for supporting this work. We also would like to acknowledge Dr. Songnan Yang of Futurewei Inc. for invaluable discussions.

REFERENCES

[1] A. P. Hu, Wireless/Contactless Power Supply:-Inductively coupled resonant converter solutions. Saarbrucken, Germany: VDM Publishing, 2009.

[2] G. Buja, M. Bertoluzzo and K. N. Mude, "Design and Experimentation of WPT Charger for Electric City Car," *IEEE Transactions on Industrial Electronics*, vol. 62, no. 12, pp. 7436-7447, Dec. 2015.

[3] B. H. Choi, V. X. Thai, E. S. Lee, J. H. Kim and C. T. Rim, "Dipole-Coil-Based Wide-Range Inductive Power Transfer Systems for Wireless Sensors," *IEEE Transactions on Industrial Electronics*, vol. 63, no. 5, pp. 3158-3167, May 2016.

[4] T. Campi, S. Cruciani, F. Palandrani, V. De Santis, A. Hirata and M. Feliziani, "Wireless Power Transfer Charging System for AIMDs and Pacemakers," *IEEE Transactions on Microwave Theory and Techniques*, vol. 64, no. 2, pp. 633-642, Feb. 2016.

[5] S. Hui, W. Zhong, and C. Lee, "A critical review of recent progress in mid-range wireless power transfer," *IEEE Transactions on Power Electronics*, vol. 29, no. 9, pp. 4500C4511, Sept 2014.

[6] S. Li, W. Li, J. Deng, T. D. Nguyen, and C. C. Mi, "A double-sided lcc compensation network and its tuning method for wireless power transfer," *IEEE Transactions on Vehicular Technology*, vol. 64, no. 6, pp. 2261C2273, June 2015.

[7] D. Ahn and P. P. Mercier, "Wireless Power Transfer With Concurrent 200-kHz and 6.78-MHz Operation in a Single-Transmitter Device," *IEEE Transactions on Power Electronics*, vol. 31, no. 7, pp. 5018-5029, July 2016.

[8] N. O. Sokal and A. D. Sokal, "Class E-A new class of high-efficiency tuned single-ended switching power amplifiers," *IEEE Journal of Solid-State Circuits*, vol. 10, no. 3, pp. 168-176, Jun 1975.

[9] Y. Han, O. Leitermann, D.A. Jackson, J.M. Rivas, and D.J. Perreault, "Resistance compression networks for radio-frequency power conversion," *IEEE Transactions on Power Electronics*, Vol. 22, No.1, pp. 41-53, Jan. 2007.

[10] D. J. Perreault, "A new power combining and outphasing modulation system for high-efficiency power amplification," *IEEE Transactions on Circuits and Systems I: Regular Papers*, vol. 58, no. 8, pp. 1713-1726, Aug 2011.

[11] L. Roslaniec, A. S. Jurkov, A. A. Bastami, and D. J. Perreault, "Design of single-switch inverters for variable resistance/load modulation operation," *IEEE Transactions on Power Electronics*, vol. 30, no. 6, pp. 3200-3214, June 2015.

[12] S. Liu, M. Liu, S. Han, X. Zhu, and C. Ma, "Tunable Class E^2 dc-dc converter with high efficiency and stable output power for 6.78 MHz wireless power transfer," *IEEE Transactions on Power Electronics*, vol. 33, no. 8, pp. 6877-6886, Aug. 2018.

[13] S. Sinha, A. Kumar and K. K. Afridi, "Active variable reactance rectifier: A new approach to compensating for coupling variations in wireless power transfer systems," *IEEE Workshop on Control and Modeling for Power Electronics (COMPEL)*, Stanford, CA, 2017, pp. 1-8.

[14] S. Cochran, F. Quaiyum, A. Fathy, D. Costinett and S. Yang, "A GaN-based synchronous rectifier for WPT receivers with reduced THD," *IEEE PELS Workshop on Emerging Technologies: Wireless Power Transfer (WoW)*, Knoxville, TN, 2016, pp. 81-87.

[15] M. Liu and M. Chen, "Dual-Band Multi-Receiver Wireless Power Transfer with Reactance Steering Network," *IEEE PELS Workshop on Emerging Technologies: Wireless Power Transfer (Wow)*, Montreal, QC, 2018, pp. 1-6.